Review

Research Progress on Catalytic Water Splitting Based on Polyoxometalate/Semiconductor Composites

Yue Wu * and Lihua Bi *

College of Chemistry, Jilin University, Changchun 130012, China
* Correspondence: wuyue17@mails.jlu.edu.cn (Y.W.); blh@jlu.edu.cn (L.B.)

Abstract: In recent years, due to the impact of global warming, environmental pollution, and the energy crisis, international attention and demand for clean energy are increasing. Hydrogen energy is recognized as one of the clean energy sources. Water is considered as the largest potential supplier of hydrogen energy. However, artificial catalytic water splitting for hydrogen and oxygen evolution has not been widely used due to its high energy consumption and high cost during catalytic cracking. Therefore, the exploitation of photocatalysts, electrocatalysts, and photo-electrocatalysts for rapid, cost effective, and reliable water splitting is essentially needed. Polyoxometalates (POMs) are regarded as the potential candidates for water splitting catalysis. In addition to their excellent catalytic properties and reversibly redox activities, POMs can also modify semiconductors to overcome their shortcomings, and improve photoelectric conversion efficiency and photocatalytic activity, which has attracted more and more attention in the field of photoelectric water splitting catalysis. In this review, we summarize the latest applications of POMs and semiconductor composites in the field of photo-electrocatalysis (PEC) for hydrogen and oxygen evolution by catalytic water splitting in recent years and take the latest applications of POMs and semiconductor composites in photocatalysis for water splitting. In the conclusion section, the challenges and strategies of photocatalytic and PEC water-splitting by POMs and semiconductor composites are discussed.

Keywords: polyoxometalates; semiconductor; water splitting catalysis; hydrogen; photocatalysis; photo-electrocatalysis

1. Introduction

Polyoxometalates (POMs) are metal—oxygen cluster compounds composed of transition metal atoms (M) and oxygen atoms (O) through corner shared and edge shared connected by MO_x polyhedra (tetrahedron, octahedron, and icosahedrons, etc.) [1]. Since the first synthesis of POM in 1826, studies on POMs have been going on for 192 years. Exception of the classical types, such as Keggin, Dawson, Anderson, Waugh, Silverton, and Lindqvist structures, a series of POM derivatives containing transition metals [2], lanthanide ions [3], organic groups [2,4] and organic metals [5] have been reported one by one. So far, POMs exhibit the diversity of composition and structure. Therefore, POMs possess many outstanding properties including stable structures, adjustable composition, dimension, and anion charge, controlled solubility in aqueous solution and organic solvents, reversible redox activity, catalytic activity, conductivity, photo- and electro-chromism, luminescence, magnetism, anti-virus, and so on. Such rich properties make POMs exhibit potential applications in the field of functional materials [6], nanotechnology [7], catalysis [8], sensing [9], analytical chemistry [10], medicine [3], and so forth.

Since the beginning of the 21st century, the earth's energy crisis and environmental problems have become more and more serious. On March 9, 2019, the United Nations Environment Programmer (UNEP) hosted the second session of the global environment problems at the science, policy, and business BBS, posted The global energy action plan for the Internet to promote global environmental governance, which mentioned that the

unreasonable energy development and utilization are the major factor of the global environment problem. According to 2016 statistics, only 4% of hydrogen comes from water splitting, and the other part comes from fossil fuels, uch as natural gas [11]. For every mole of hydrogen produced, four moles of carbon dioxide are also produced [12]. Consequently, if the traditional energy sources could be replaced by the clean energy, the pollution of fossil fuel emissions would be cut down and the increase in the earth's average atmospheric temperature would be effectively controlled. So far, the development and utilization of energy are changing from the traditional non-renewable energy to the renewable clean energy led by solar energy. With the exploitation of solar energy, the POMs have been paid more and more attention due to their intriguing optical properties. The application classification of POMs utilizing solar energy mainly includes solar cell [13], artificial simulation of photocatalytic hydrogen generation [14], degradation of organic dye wastewater [15], photo-electrocatalysis [16] and photoluminescence [17].

Light sensitivity of POMs was reported by Rindl as early as 1914. The photocatalytic chemistry of POMs was not mentioned until the 1980s. In 1985, the Hill's group studied the photocatalytic chemistry of POMs, and a reasonable model was proposed to explain the relationship between the light absorption wavelength of POM-organic matrix system and the photochemical reaction system [18]. The starting point of POMs as photocatalyst is that the POMs possess the similarity to semiconductor metal oxides, such as titanium dioxide (TiO_2): they have similar chemical composition and electronic property; that is, they both contain transition metal elements with d^0 electron configuration [19,20] and oxygen atoms. Based on molecular orbital theory, for POM molecules, the light absorption process is ascribed to the electrons migration from the HOMO (highest occupied orbital) to the LUMO (lowest vacant orbital); that is, the irradiation of POM molecules under ultraviolet (UV) light source causes the move of electrons in the oxygen atom (O_{2p}) on the M–O–M (M=W, Mo) bridge bond to M_{5d} transition metal vacant orbital: O→M called charge-transfer transition. Further, the energy gap for the LUMO-HOMO of the POMs is the same as the CB (conduction band) to VB (valence band) of $TiO_2¬$, for example, the LUMO-HOMO of $W_{10}O_{32}{}^{4-}$ is 2.9–3.0 eV and the energy gap (Eg) of TiO_2 is 3.2 eV. According to the representative of semiconductor as photocatalyst, the electrons jumped to M_{5d} orbital are considered as photogenic electrons whilst the vacant orbital left by electron transition on the O_{2p} orbit can be regarded as photogenic hole, as shown in the following formula:

$$POM + h\nu \boxed{\leftrightarrow} POM * \boxed{\leftrightarrow} POM\left(e^- + h^+\right) \tag{1}$$
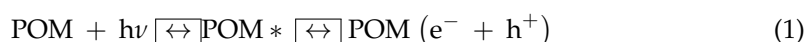
Thereinto, POM* represents the POM in the excited state

The two excited states formed by photoexcitation for POMs and TiO_2 have similar redox properties, for instance the redox potential of Keggin-type POMs in the excited state is 2.63 V, while that of TiO_2 in the excited state is 2.62 V [21]. Such comparison indicates that both of their excited states have strong oxidation capacity. Many organic chemical reactions, which are thermodynamically difficult to be performed or can only be performed under harsh conditions, can be successfully carried out under mild experimental conditions by photocatalysis of POMs or TiO_2 [22–24]. Therefore, POMs have the characteristics of semiconductor metal oxides and can be used as excellent photocatalysts.

Compared with metal, the band of semiconductor is discontinuous, and there is a forbidden band between the VB and CB [25]. Most of the semiconductors used as photocatalysts are metal oxides and sulfides, which generally have a wide band gap, sometimes called wide band gap semiconductor. The band gap diagram of a common semiconductor material is shown in Figure 1 below. For example, TiO_2 and its derivatives play an important role in photochemistry. The main reason is that its Eg at pH 1 is 3.2 eV (usually the Eg of 3 eV is used as the boundary dividing the semiconductor and the insulator, and Eg less than 3 eV is called the semiconductor, but this division is not absolute). The structure, properties, and applications of TiO_2 are introduced in detail by Henderson [26] and Kukovecz et al. [27]; CdS with Eg of only 2.4 eV is solar energy available and a well-studied catalyst showing excellent hydrogenation activity but limited by its

susceptibility to photocorrosion [28]. The light absorption threshold of the semiconductor is related to the band gap in equation (1) [29], from (1) it can be seen that the absorption wavelength threshold of wide band gap semiconductors commonly used is mostly in the UV region.

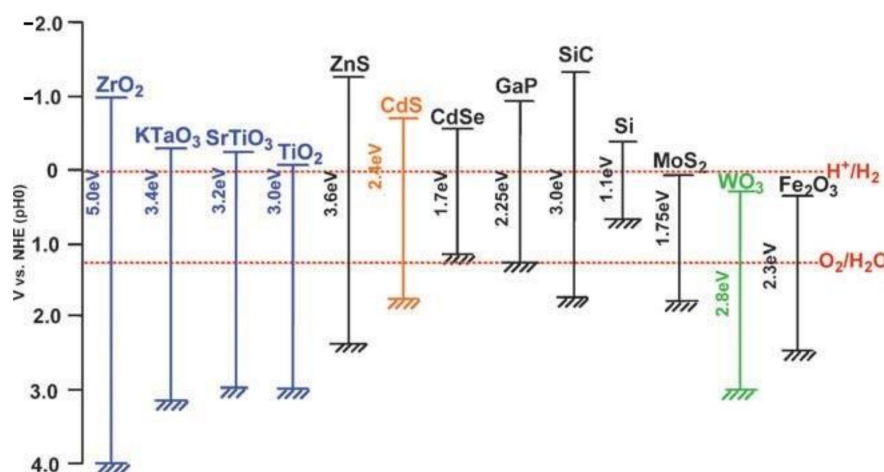$$\lambda g \ (nm) = 1240 / Eg \ (eV), \tag{2}$$

Figure 1. The band gaps of some semiconductors [30].

The photocatalytic properties of semiconductors have been confirmed by many studies [31], but from the efficiency of using sunlight, there are still the following main defects: first one is that the light absorption wavelength range for the semiconductor is narrow, mainly in the UV region, the proportion of using sunlight is low; another one is that the semiconductor carrier recombination rate is very high, so the quantum efficiency is low. Considering the drawbacks above, the scholars have studied the modification of semiconductor photocatalysts in the hope of improving excitation charge separation and inhibiting carrier recombination to enhance quantum efficiency; extending the wavelength range of the light; improving the stability of photocatalytic materials, etc. The modification methods for the semiconductors involve the complex semiconductors, for example, TiO_2-CdS, can not only improve the charge separation effect of the system, but also expand its spectral response range [32]; quantum effect is used to change the band gap width of semiconductor materials by adjusting the particle size of the semiconductor materials [25] (for example, when the diameter of CdS particles is 26 Å, the band gap width increases from 2.6 to 3.6 eV [33–35]); the deposition of precious metals [36–40] on the surface of the semiconductor can rapidly capture and transfer excited electrons and inhibit carrier recombination doping of semiconductor with some metal ions [41,42] introduces defect position into semiconductor lattice, affects electron-hole pair recombination, and effectively improves the photon quantum efficiency; semiconductor photosensitization [43,44], and other methods.

Opposed to traditional semiconductor materials, such as TiO_2, CdS, Co_3O_4, ZnO, etc., POMs have unique advantages, such as POMs have a wide variety of types and the adjustable property of band gap (the band gap of POMs is in the range of 2.48–3.44 eV); thus, the light absorption range of POMs could be broadened from UV to visible light region (the absorption wavelength is in the range of 360–500 nm, as shown in Figure 2). At the same time, POMs are good electron acceptors, when combined with wide band gap semiconductors, on the one hand, the wavelength range of absorbed light can be extended as far as possible and visible light can be fully utilized; on the other hand, POMs can capture and transfer photogenerated electrons from semiconductors, excite charge separation, and inhibit carrier recombination to improve quantum efficiency. In 2003, Choi et al. pointed out that POMs can be used as an electronic medium to generate electrons from TiO_2 in solution and transfer to the inert electrode with photoelectric chemical device [45].

In addition, POMs also have redox reversibility and excellent catalytic performance, which can keep their structure unchanged while accepting electrons. Therefore, POMs have broad development value and application prospect in photocatalysis and photoelectric conversion [46–48].
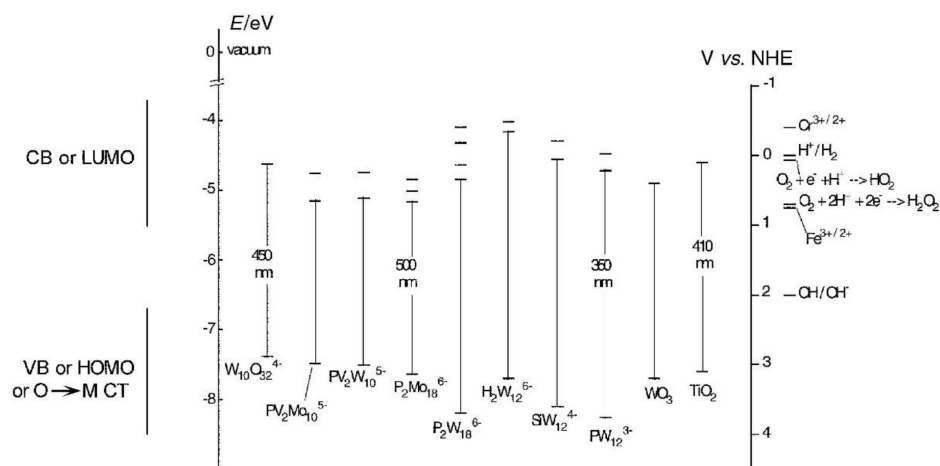

Figure 2. HOMO and LUMO of POMs [48].

It is well known that photosynthesis is the process to convert carbon dioxide and water in green plants and algae into carbohydrates and oxygen under sunlight. Mn_4O_5Ca is the reactive center of PSII in photosynthesis [49]. In the long history of human development, people are always getting inspiration from the nature. The invention of airplane comes from the research on birds, the invention of waterproof fabric comes from the hydrophobic effect of lotus leaves, and the research on photocatalysis and PEC of water splitting to hydrogen/oxygen comes from the photosynthesis of natural green plants and algae. Thus, artificial photosynthesis is the process to synthesize suitable materials to replace photosynthetic reactive centers so that water can be efficiently converted into hydrogen and oxygen by the assistance of the synthesized materials when exposed to solar [50–52]. POMs containing W^{VI}/Mo^{VI} involve the similar structure with Mn_4O_5Ca and has good catalytic performance [14] as homogeneous and heterogeneous catalysts [53]; thus, POMs are considered as the potential photosynthetic reactive centers for the artificial photosynthesis.

Whether the PEC water splitting catalyst has practical application value depends on the following points: first, whether the band gap width is in the recombination range, the closer to 2.53 eV [54], the higher the photoelectric conversion efficiency of sunlight; the second is whether the band position meets the requirements of hydrogen evolution and oxygen evolution Minimum potential requirements; third, is whether the photo-generated electron-hole recombination rate is relatively low; fourth, is whether the charge carrier transport rate is fast enough; and fifth, is whether the catalyst stability is good. The development of semiconductor metal oxides has been a long time. The absorption and catalytic properties of semiconductor materials for light have been proved. However, the limitations of semiconductor materials make it difficult for them to be widely used. Consequently, the materials on the combination of POMs and semiconductors are developed by some researchers to improve their synergistic catalytic performance for water splitting. This is a new field, which needs more researchers' attention and understanding. Under this situation, in this review, we will be centered on the research progress of POMs and semiconductor composite materials in the field of photocatalytic and PEC water decomposition in recent ten years. Among them, heterogeneous reactions using POMs as the catalysts are mainly discussed. In Scheme 1, we provide the timeline of important breakthroughs for POMs-based semiconductor compounds in Photocatalytic and PEC water splitting catalysis. It will be introduced in more detail later.
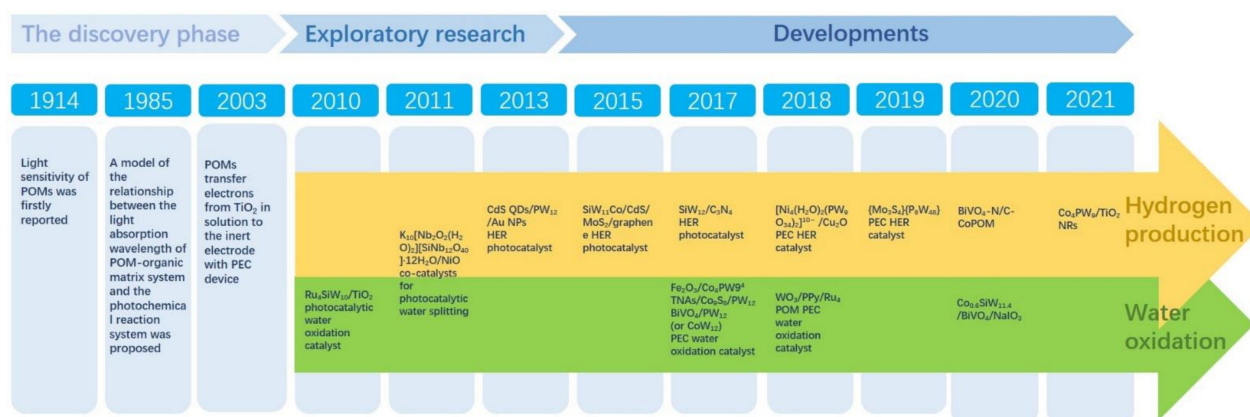
Scheme 1. Timeline of important breakthroughs for POMs-based semiconductor compounds in Photocatalytic and PEC water splitting catalysis.

2. Recent Advances and Applications

In recent years, the research on POMs mainly focuses on combining POMs with semiconductor materials to prepare synergistic functional composite materials applied in the field of photocatalysis, solar cells, degradation of organic dye in waste water, artificial simulation of photocatalytic hydrogen production and PEC water-splitting, etc. In 2000, Yoon et al. prepared TiO_2-POMs complex, which was proved that the photocatalytic performance for methyl orange was significantly improved [55]. In 2007, Shannon et al. [56] used TiO_2/POMs system on the photocatalytic oxidation of methanol, and it was found that the photocurrent of the composite system was higher 50 times more than that of TiO_2 alone due to the presence of POMs. The reason is ascribed to that the light generated electrons on TiO_2 can be captured in the CB by POMs, leading to the improvement of the photocatalytic performance.

2.1. Photocatalytic Water-Splitting

Solar energy, as a kind of renewable energy, is not only widely used in nature, such as photosynthesis, but also attracts many researchers to study photocatalysts, so as to realize the conversion from solar energy to chemical energy [14,30,57–68]. This is determined by the urgent need for environmentally friendly and clean energy in today's society. Most organisms on earth are directly or indirectly dependent on natural photosynthesis. Converting sunlight into 'wireless electricity' is the main step in photosynthesis [69–71]. "The anodic charge of the wireless current is used at the PSII OEC (oxygen evolving complex) to oxidize water to oxygen, with the concomitant release of four protons; The cathodic charge of the wireless current is captured by PSI to reduce the protons to 'hydrogen', which is temporarily stored in the form of NADPH (reduced biological hydrogen) and ATP" [14] (adenosine triphosphate). In nature, the composition of PSII OEC is confirmed as Mn_4O_5Ca [72]. During the photosynthesis process, in PSII system OEC catalytically oxidize water molecules to generate O_2. For this catalytic oxidation reaction, the catalyst undergoes a cycle process from S0 to S4 [73]. Therefore, it is required that the catalyst should be stable and easily detected. Based on the structural feature of OEC, the preparation of the catalysts with similar structure to Mn_4O_5Ca becomes a hot issue in present research. Due to the reversible redox property and adjustable composition and structure, POMs have become potential candidates to simulate PSII OEC catalyst [63,64,74–80].

At present, the photocatalytic chemistry of POMs is mostly concentrated in the homogeneous system, and there are relatively few studies on the heterogeneous system.

For the catalytic oxidation reaction of water molecules, two difficult problems need to be addressed: one is that the removal rate of photogenic hole is slow; another is that photogenic electron-hole pair recombination is faster. In order to solve two issues above,

many researchers have contributed their efforts to perfect the composite and structure of catalysts.
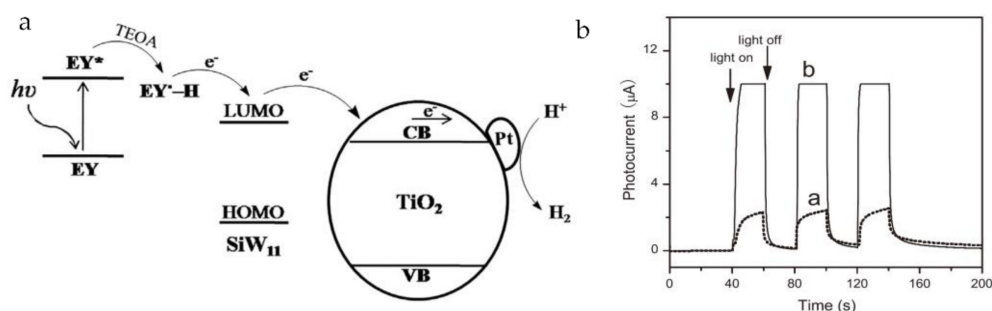
2.1.1. POMs Modified TiO$_2$ Photo-Catalyst

In 2010, Orlandi et al. [81] synthesized a hybrid material by combining tetraruthenium POM water oxidation catalyst ([Ru$_4$(μ-O)$_4$(μ-OH)$_2$(H$_2$O)$_4$(g-SiW$_{10}$O$_{36}$)$_2$]$^{10-}$ (1)) in Figure 3, with TiO$_2$, which used the high negative charge of one and its benefit in close contact with the positively charged TiO$_2$ to realize the goal of fast hole scavenging from photogenerated Ru$^{(III)}$ polypyridine complexes, both in homogeneous solution and at a sensitized nanocrystalline TiO$_2$ surface under 8 ns pulses of 355 nm light from a frequency tripled Nd:YAG laser.
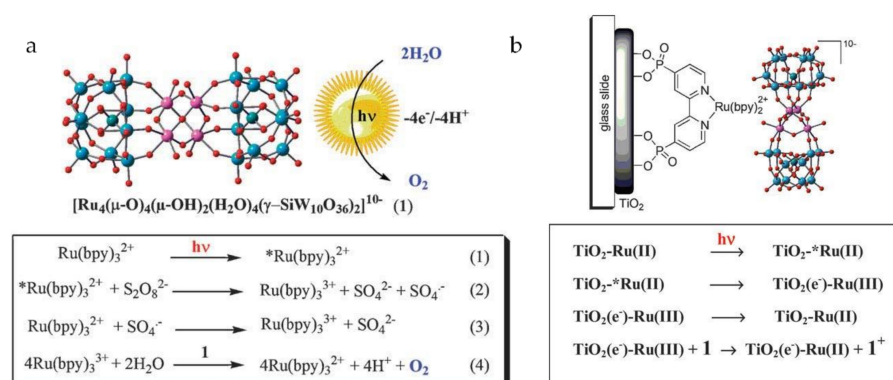
Figure 3. (**a**) Water oxidation by photogenerated Ru(bpy)$_3$$^{3+}$, using 1 as catalyst and persulfate as sacrificial electron sink. (**b**) Reaction of catalyst 1 with Ru$^{(III)}$ species photogenerated by electron injection into nanocrystalline TiO$_2$ layer [81].

As a good electron acceptor, POMs can be used not only in the composite materials containing semiconductor to reduce the combination speed of photogenerated electron-hole pairs, but also in the hydrogen production catalyzed by dye-sensitized solar energy to extend the life of sensitizer and increase its stability by transferring the electrons of sensitizer. In 2013, Liu et al. [82] designed a dye-sensitized solar cell involving the composite material of lacunary Keggin-type POMs SiW$_{11}$O$_{39}$$^{8-}$ (SiW$_{11}$) and semiconductor TiO$_2$, using Eosin Y (EY) dye as sensitizer and Pt as co-catalyst. This cell showed the improvement of the hydrogen production efficiency due to the presence of SiW$_{11}$. Figure 4 displays the schematic diagram of the conjecture and the photo response of SiW$_{11}$ to the catalyst under light conditions. "Under the optimal conditions, an average apparent quantum yield of 11.4% was obtained during 20 h irradiation (λ> 420 nm)."


Figure 4. (**a**) Probable mechanism of hydrogen production in EY sensitized SiW$_{11}$/TiO$_2$. (**b**) The photocurrent responses of (**a**) EY-TiO$_2$ and (**b**) EY-SiW$_{11}$/TiO$_2$ electrode under 520 nm visible light irradiation [82].

2.1.2. POMs Modified CdS Photo-Catalyst

Because Co [83], Ni [84] and Mn-containing POMs [85] alone exhibit a certain catalytic activity for water splitting, the combination of such compounds with semiconductor components can play expected synergistic catalytic effect. In 2013, Xing et al. [86] prepared a kind of molecular self-assembled nano hybrids (Cadmium sulfide quantum dots/$H_3PW_{12}O_{40}$/gold nanoparticles, CdS QDs/PW_{12}/Au NPs) which can efficiently collect visible light and show synergistic photocatalytic activity in the production of hydrogen light. Among them, the PW_{12} encapsulated molecules and bridged molecules not only successfully achieved strong coupling of different nanoparticles, but also enhanced the electron transfer between the various components of the nanohybrid. In 2015, Liu et al. combined the semiconductor CdS with Co-containing POM ($Na_6SiW_{11}O_{39}Co^{(II)}(H_2O)$, $SiW_{11}Co$) to form the composite material CdS/$SiW_{11}Co$ [87]. Further, in order to better inhibit photogenerated electron-hole pair recombination, nanoscale MoS_2/graphene(M/G) composite was introduced as a reduction auxiliary catalyst. In the whole system, without the participation of precious metals, the cost of photocatalytic hydrogen evolution catalyst can be effectively reduced. Moreover, the activity of CdS is increased up to 21.3 times with 1 wt% $SiW_{11}Co$ and 5 wt% M/G loaded compared to CdS alone. The result shows that the as-prepared sample reaches a H_2 evolution rate of 1.7 mmol h^{-1}.

In 2016, Bu et al. [88] used the MOF (UiO-67) to combine 12-tungstosilicic acid ($H_3SiW_{12}O_{40}$, SiW_{12}) with semiconductor CdS to produce a photocatalyst SiW_{12}@Zr-based metal—organic frameworks/MoS_2/reduced graphene oxide-CdS (SiW_{12}@UiO-67/M/G-CdS), in which CdS was selected as the photocatalytic activity center due to its narrower band gap (2.4 eV), and SiW_{12}@ UiO-67 as the supporting matrix. Moreover, in order to improve the photocatalytic activity for hydrogen production from multiple perspectives, MoS_2/reduced graphene oxide (M/G) component as the co-catalyst was introduced to the hybrid material above. The performance study of photocatalytic hydrogen evolution indicates that the optimum H_2 production rate is 1.27 mmol·h^{-1} when the material composite of SiW_{12}@UiO-67/M/G-CdS contains 30 wt% SiW_{12}@UiO-67 and 5% M/G. The compared results are shown in Figure 5, it can be seen that the heterostructure hybrid composite SiW_{12}@UiO-67/M/G-CdS displays enhanced photocatalytic activity. Such observation might be ascribed to the effective heterostructure feature between each component and SiW_{12}@UiO-67 with large specific surface area. Additionally, SiW_{12} is inserted into the porous UiO-67 to increase the ability promoting transfer electrons which accelerated the separation of photogenerated electrons and holes and suppressed the fast recombination of CdS charge carriers.
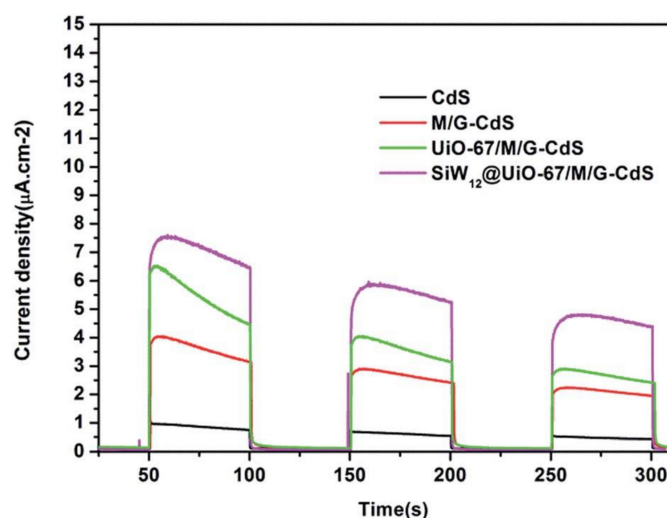
Figure 5. Transient photocurrent responses of the materials involving CdS, M/G-CdS, UiO-67/M/G-CdS, and SiW_{12}@UiO-67/M/G-CdS under visible light irradiation [88].

In 2018, Zhai et al. [89] used hydrothermal synthesis method to introduce g-C$_3$N$_4$ and POM (Na$_6$K$_4$[Ni$_4$(H$_2$O)$_2$(PW$_9$O$_{34}$)$_2$]·32H$_2$O, Ni$_4$(PW$_9$)$_2$) into CdS to obtain a photocatalytic hydrogen production system. At the same time, in order to improve the electrical conductivity of the catalyst and enhance its stability, polypyrrole (PPy), which has high electrical conductivity and is easy to prepare, relatively low cost, was also incorporated. The hydrogen evolution rate of the composite catalyst of Ni$_4$(PW$_9$)$_2$/g-C$_3$N$_4$/PPy/CdS, in its best condition, tendency for 1.321mmol·h^{-1}, slightly better than that of SiW$_{12}$@UiO-67/M/G-CdS [88].

2.1.3. POMs Modified Co$_3$O$_4$ Photo-Catalyst

In 2016, Lan et al. [90] compounded Keggin-type POM (H$_3$PW$_{12}$O$_{40}$, PW$_{12}$) with low-cost Co$_3$O$_4$ on Metal—Organic Framework (MOF) with hollow, porous structure, low density, large specific surface area and good load capacity of MOF by sintering, in which the material of PW$_{12}$ modified MOF was used as a precursor. Such prepared hybrid materials effectively improved the specific surface area of the catalyst and exposed more active sites, thus enhancing the catalytic performance of the catalyst for photocatalytic water oxidation. The TOF (turnover frequency) of PW$_{12}$/(Co$_3$O$_4$)$_{12}$ can reach $1.11*10^{-3}$ s^{-1}, which is the highest value among the reported materials based on Co$_3$O$_4$ for visible light-driven water oxidation.

2.1.4. POMs Modified g-C$_3$N$_4$ Photo-Catalyst

In addition to the traditional semiconductors mentioned above used as photocatalysts, graphitic carbon nitride (g-C$_3$N$_4$) has been recognized as a new non-metallic photocatalytic material because it has a wider range absorption spectrum and can play a photocatalytic role only under ordinary visible light without the need for ultraviolet light. Wang et al. [91] confirmed that g-C$_3$N$_4$ non-metallic semiconductor can catalyze water splitting to produce hydrogen and oxygen under light for the first time in 2009. In 2017, Yan et al. [92] prepared a series of composite materials (POM/ g-C$_3$N$_4$) containing Keggin-type polyoxoanion (SiW$_{12}$O$_{40}$$^{4-}$, PW$_{12}O_{40}$$^{3-}$, PMo$_{12}O_{40}$$^{3-}$) and g-C$_3N_4$ and used them as photocatalysts for water splitting. The investigated results indicate that thus-prepared composite materials show high photocatalytic activity for H$_2$ generation under visible light irradiation. The H$_2$ evolution rate of SiW$_{12}$/C$_3$N$_4$ is 484 µmol g^{-1} h^{-1} as shown in Figure 6, which is about 1.46 times higher than that of pure g-C$_3$N$_4$ (332 µmol g^{-1} h^{-1}). The experimental results confirm that g-C$_3$N$_4$ has photocatalytic hydrogen evolution capability. All POMs can be used as electron traps, which can effectively inhibit the recombination of g-C$_3$N$_4$ photogenerated carriers. When POM/g-C$_3$N$_4$ is excited by visible light, the photogenerated electrons of g-C$_3$N$_4$ are captured by POMs, thus the spatial separation of photogenerated carriers is promoted, but their trapping ability may be related to their band gap and redox properties.
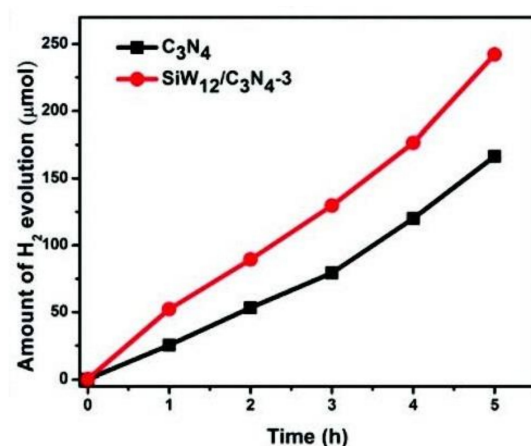

Figure 6. Comparison of the hydrogen generation rate of the hybrid SiW$_{12}$/C$_3$N$_4$-3 with g-C$_3$N$_4$ under visible light irradiation [92].

2.1.5. POMs Modified Other Semiconductors Photo-Catalyst

In 2011, Zhang et al. [93] tried to adjust the structure of the material itself to improve the performance of photocatalyst. For this purpose, the authors synthesized a new structure containing niobic POM, $K_{10}[Nb_2O_2(H_2O)_2][SiNb_{12}O_{40}]\cdot12H_2O$ (2), which is compared with the previously reported containing niobic POM, $Na_{10}[Nb_2O_2][SiNb_{12}O_{40}]\cdot xH_2O$ (3), the main difference on structure between them is that in compound 3 Nb^{5+} shows the octahedral coordination geometry whereas in compound 2 Nb^{5+} is seven-coordinated by four O^{2-} ions from the $[SiNb_{12}O_{40}]$, two bridging O^{2-} ions and a water molecule. Such unusual geometry leads to an extreme distortion of O–Nb–O bond angles on the bridging dimer $[Nb_2O_2(H_2O)_2]^{6+}$ changing from ~73 to 122°. Perhaps this distorted NbO_7 unit could give a better separating charge effect than the NbO_6 octahedron. Therefore, the photocatalytic H_2 evolution efficiency for 0.5% Pt-loaded compound 2 reached 2100 mol/h/g (as shown in Figure 7a) with Xe lamp of 300W, which is better than H_2 evolution efficiency (1205 mol/h/g) for 0.5% Pt-loaded compound 3. Accordingly, the creation of an open metal site might be an effective strategy to achieve more efficient photocatalysts. Moreover, in this paper, the authors also combined compound 2 with semiconductor NiO as co-catalysts to study its overall photocatalytic water splitting property in pure water, as shown in Figure 7b, the rates of H_2 and O_2 evolved under UV irradiation are 222 and 97 μmol h^{-1} g^{-1}, respectively. The study results further demonstrate that POM is feasible used to photocatalytic overall water-splitting reaction.
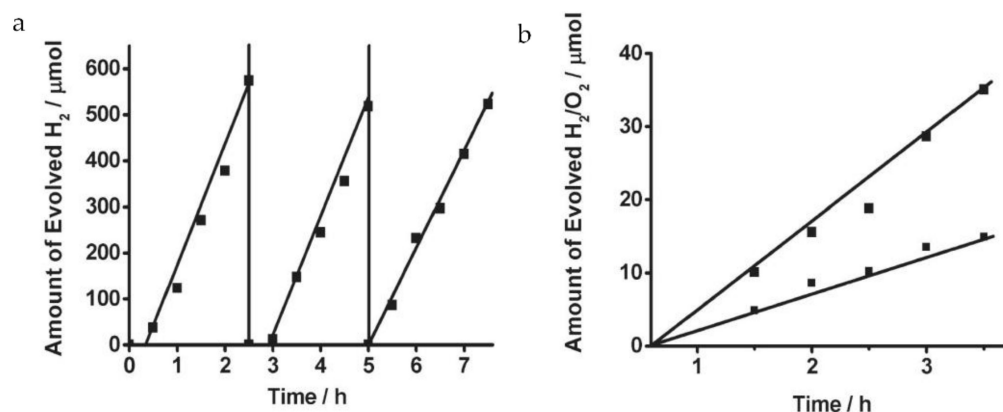
Figure 7. (**a**) Time course of H_2 evolution from 100 mg of 0.5% Pt loaded photocatalyst 2 under UV irradiation in 270 mL of 20% methanol aqueous solution. (**b**) Time course of overall water splitting from 50 mg of 0.5% NiO-loaded photocatalyst 2 under UV irradiation in 270mL of pure water. Reprinted with permission from [93]. Copyright (2011) American Chemical Society.

In 2020, combing cobalt containing POM $K_4H_{1.2}[Co_{0.6}(H_2O)_{0.6}SiW_{11.4}O_{39.4}]15H_2O$ with $BiVO_4$, Dong et al. [94] studied the visible light driven water oxidation catalytic performance of the co-catalyst with $NaIO_3$ as sacrificial electron acceptor, and discussed the stability and catalytic effect of the co-catalyst in a wide pH range of 1–7. Among them, cobalt containing POM was stable at pH 4. The highest oxygen generation rate is about 11 μmol / h and O_2 yield is 21.8%. It should be noted that under the conditions of pH 1–3 and 6–7, the particles CoOx generated in the water oxidation reaction catalyzed from $K_4H_{1.2}[Co_{0.6}(H_2O)_{0.6}SiW_{11.4}O_{39.4}]15H_2O$ and $BiVO_4$, which would reduce the catalytic efficiency.

Table 1 lists POMs-based semiconductor compounds in Photocatalytic water splitting and is organized in a chronological format.

Table 1. Summary of POMs-based semiconductor compounds in photocatalytic water splitting.

No.	Cocatalyst	Solution/pH	Ratio (wt %)	Light Source	H_2 (O_2) Evolution Efficiency/TOF	References
1	Ru_4SiW_{10}/TiO_2	-	-	Osram XBO150W/1 OFR xenon lamp Excitation, 532 nm, FWHM 8 ns	-	Orlandi et al. (2010) [81]
2	$K_{10}[Nb_2O_2(H_2O)_2][SiNb_{12}O_{40}]\cdot 12H_2O/NiO$	pure water (pH 7)	99.5:0.5	Xe lamp of (300W)	222 (H_2)/ 97 (O_2) μmol h^{-1} g^{-1}	Zhang et al. (2011) [93]
3	CdS QDs/PW_{12}/Au NPs	0.1 M Na_2S and 0.1 M Na_2SO_3 aqueous solution	94:6	Xenon lamp (500 W) ($\lambda >$ 420 nm)	ca.550(H_2) μmol h^{-1} g^{-1}	Xing et al. (2013) [86]
4	SiW_{11}/TiO_2/EY/Pt	pH 7	-	Hg lamp (400 W) ($\lambda >$ 420 nm)	65.2 mmol h-1 average apparent quantum yield 11.4%	Liu et al. (2013) [82]
5	SiW_{11}Co/CdS/MoS_2/graphene	30 vol% lactic acid aqueous solution	1:94:5	Xe lamp (300 W) ($\lambda >$ 400 nm)	1.7 mmol h^{-1}	Liu et al. (2015) [87]
6	$PW_{12}/(Co_3O_4)_{12}$	Na2SiF6/NaHCO3 buffer solution/pH 6.0	-	300 W Xe lamp equipped with a long-pass filter (420 nm cutoff)	TOF1.11*10-3·s^{-1}	Lan et al. (2016) [90]
7	SiW_{12}@UiO-67/M/G-CdS	30 vol% lactic acid aqueous solution	30:65:5	300 W Xe lamp ($\lambda >$ 400 nm)	1.27 mmol·h^{-1}	Bu et al. (2016) [88]
8	SiW_{12}/C_3N_4	1.0 wt% Pt (H2PtCl6) triethanolamine (30 mL) and deionized water (90 mL)	-	300 W Xe lamp ($\lambda >$ 400 nm)	484 μmol 1 h^{-1} g^{-1}	Yan et al. (2017) [92]
9	$Ni_4(PW_9)_2$/g-C_3N_4/PPy/CdS	0.35 M Na_2SO_3 and 0.25 M Na_2S aqueous solution	-	300 W xenon arc lamp ($\lambda =$ 420 ~ 800 nm)	1.321mmol·h^{-1}	Lan et al. (2018) [89]
10	$K_4H_{1.2}[Co_{0.6}(H_2O)_{0.6}SiW_{11.4}O_{39.4}]15H_2O$/BiVO_4/NaIO_3$	sodium acetate and acetic acid (100 mM)/pH 4.0	-	LED light source 100 mW cm^{-2} ($\lambda =$ 420 nm)	(O_2) ca.10 μmol 1 h^{-1}	Dong et al. (2020) [94]

2.2. Photo-Electrocatalysis (PEC) for Water-Splitting

The principle of PEC for water-splitting is to take semiconductor as photo-electrocatalyst to produce photogenerated electrons and holes under the radiation of the sunlight, and then decompose water into hydrogen and oxygen by the action of external electric field, thereby realize the conversion from solar energy to chemical energy. PEC is a special existence between photocatalysis and electrocatalysis. Taking TiO_2 as an example, the reaction mechanism of photoelectric electrode is introduced as follow: when enough light hits TiO_2 to produce photogenerated electrons and holes whilst a certain voltage or current is applied to the optical electrode, which can force the generated photoelectric current to flow to the opposite electrode, thus reducing the recombination of photogenerated electron-hole pair [95].

2.2.1. Principle of PEC for Water-Splitting

As water is a weak electrolyte, it can ionize to produce hydrogen ions (H^+) and hydroxyl ions (OH^-) [96]. Semiconductors can produce photogenerated electrons and holes after absorbing light, on the one hand, photogenerated electrons can reduce hydrogen ions into hydrogen, on the other hand, photogenerated holes can oxidize water molecule into oxygen. Among them, the reduction electrode potential of H^+ is 0V, and the oxidation potential of water molecule is 1.23V. Therefore, it is theoretically understood that it takes 1.23 eV of energy to decompose a water molecule into hydrogen and oxygen. To sum up, the whole process of photocatalytic decomposition of water molecule by semiconductor can be divided into three steps:

Light absorption by a semiconductor: when the semiconductor is illuminated, the photogenerated electrons jump directly from the valence band to the conduction band, while the photogenerated holes stay in the valence band.

The migration of photogenic charges: under the action of external electric field, photogenerated electron-hole pairs are separated, photogenerated electrons migrate to the photocathode surface, while photogenerated holes remain on the photoanode surface.

Redox reaction: H^+ ions are reduced to H_2 by photogenerated electrons at the photocathode. Photogenic holes on the surface of the photoanode oxidize H_2O to O_2.

2.2.2. POMs Modified TiO_2 Photo-Electrocatalyst

According to the U.S. Department of Energy (DOE), the 2020 target for the cost of PEC hydrogen is USD 5.70 kg, down from USD 17.30 kg in 2015, while the ultimate target is USD 2.10 kg [97]. POM has a large quantity, low price, and cost advantage, but the photoelectric property of pure POMs is limited, so researchers often associate POMs with semiconductor materials such as TiO_2, ZrO_2, Ta_2O_5, etc. [98–101]. Due to the reversible redox property of POMs, the introduction of POMs to the semiconductor materials can get the enhanced synergistic function. So far, the saturated and substituted POMs have been compounded with the semiconductor materials. Choi's group [16] combined a POM ($PW_{12}O_{40}^{3-}/PW_{12}O_{40}^{4-}$) couple with TiO_2 earlier. As shown in Scheme 1, in 2003, by monitoring the photocurrent generation, the electron transfer mediating ability of POMs in aqueous solution or TiO_2 suspension under UV illumination was directly demonstrated, and TiO_2 was the first anode material used to demonstrate PEC water splitting [12]. The band gap of TiO_2 is 3.2 eV, and the main light absorption range is 387 nm, which belongs to near ultraviolet light. As an anode, it absorbs photon energy and excites electrons to transition to the conduction band. The photogenerated holes oxidize the water and finally produce oxygen. The entrainment position is about -3.52 eV [102]. According to the common POMs HOMO-LUMO spectrum in Figure 2, It is speculated that the POMs with a CB position lower than that of titanium dioxide is easy to deprive the excited electrons from TiO_2, thereby transferring them to the internal circuit, reducing the photo-generated electron recombination rate and improving the catalytic efficiency.

In 2010, Sun et al. [95] utilized layer by layer (LBL) self-assembly method to deposit PW_{12} ($H_3PW_{12}O_{40}$) and TiO_2 nanoparticles on the ITO substrate to obtain PW_{12}/TiO_2 composite photoanode, which was applied to photoelectric materials, showing improved

the photoelectric performance for the electrode. Under the chopped UV light irradiation in 0.1 M Na_2SO_4 at a constant bias of 0 V, a nearly twofold increase in the photocurrent for the $(PW_{12}/TiO_2)_3$ film as compared to that of the $(PSS/TiO_2)_3$ film was found. In 2012, the same research group [103] fabricated the composite films containing $[(C_4H_9)_4N]_4SiW_{12}O_{40}$ (SiW_{12}) and ZnO on photoanode by electrodeposition avenue. The investigation indicated that thus-prepared photoanode containing POM/ZnO showed the enhanced ca. 70% photocurrent than ZnO films alone.

In 2013, Xu et al. [104] combined $[\{Ru_4O_4(OH)_2(H_2O)_4\}(\gamma\text{-}SiW_{10}O_{36})_2]^{10-}$ water oxidation catalyst with semiconductor metal oxides ZrO_2, TiO_2, and SnO_2 and sensitizer $[Ru(bpy)_2(dpbpy)]^{2+}$ (P2) to construct triadic photoanodes [105]. Photochemical tests showed a significant increase in visible induced photocurrent (> 100%) compared to the TiO_2-P2 electrode without the POM catalyst, suggesting light-driven water oxidation, and a significant improvement in their quantum efficiency (ca. 0.2%), particularly in hydrolysis stability.

Three composite materials containing POMs and semiconductors above were mainly applied to solar cells and the investigated results indicated that their combination achieved higher photoelectric conversion efficiency. Accordingly, such composite materials were further utilized to decompose water molecules to produce hydrogen energy and oxygen.

In 2015, Hill et al. [106] immobilized the POMs $[Ru^{IV}_4O_5(OH)(H_2O)_4(\gamma\text{-}PW_{10}O_{36})_2]^{9-}$ (Ru_4P_2) and $[Ru^{IV}_4(OH)_2(H_2O)_4(\gamma\text{-}SiW_{10}O_{34})_2]^{10-}$ (Ru_4Si_2) with water oxidation catalytic activity on TiO_2 nanoparticles with silanization to prepare nanoporous electrodes Ru_4X_2-TiO_2/FTO (X = P and Si). Multiple techniques were utilized to characterize thus-prepared electrodes and prove that the silanization is effective for immobilizing Ru_4X_2 on the surfaces of nanoparticle modified electrodes, which not only maintains the catalytic activity for water oxidation, but also affords enough concentrations of Ru_4X_2 immobilized on the nanoparticle modified electrodes for characterizing the water oxidation catalysts (WOCs) before and after the catalytic reaction by spectroscopic or electron microscopic technique. Further, the prepared composite electrodes were used in photoelectrochemical systems to investigate photo-electrocatalysis of water splitting. The results indicate that the photocurrent density produced by the composite electrodes $Ru_4X_2-TiO_2$/FTO for water oxidation is sustainably increased compared to TiO_2/FTO (see Figure 8) and the prepared electrodes $Ru_4X_2-TiO_2$/FTO exhibit high stability due to the treatment of the cationic silylating agent on TiO_2.
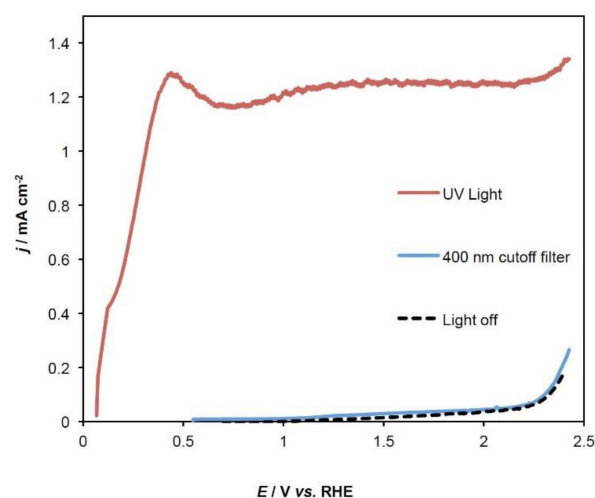
Figure 8. The comparisons of linear scan voltammetry of Ru_4P_2-TiO_2 electrodes under UV light illumination, 400 nm cutoff filter, and light off. Conditions: 0.1 M KNO_3 electrolyte, pH 10, adjusted with KOH, 100 mV/s scan rate, 0.13 W/cm^2 UV light power density. Reprinted with permission from [106]. Copyright (2015) American Chemical Society.

In order to improve the conductivity of photo-electrocatalyst, graphene materials with better conductivity for photo-electrocatalysis were considered. In 2016, Peng et al. [107] combined POMs with graphene (GO) and TiO_2, and the photoelectric conversion performance of the composite film was studied. The research results show that the composite membrane $GO–TiO_2–PW_{12}–TiO_2$ has better photoelectric response effect and has a good prospect in the future application of photoelectric switches.

In 2017, Jeon et al. [108] used layered self-assembly (LBL) technology to combine POMs($[Co_4(H_2O)_2(PW_9O_{34})_2]^{10-}$, Co_4PW_9) with four kinds of polyelectrolytes (PEs) to form multilayer PEs/POMs and assembled them into three kinds of semiconductor materials (Fe_2O_3, $BiVO_4$, and TiO_2) to prepare photoelectric anode materials, as shown in Figure 9a. The band gap of alpha-Fe_2O_3 is similar to 2.2–2.3 eV value. As a result of which Fe_2O_3 is capable of absorbing a large portion of the visible solar spectrum (absorbance edge similar to 600 nm). [109] Among the four PEs positively charged materials, b-PEI and POMs display the greatest improvement on the photocatalytic performance of Fe_2O_3 after assembly, and the photo-electrocatalytic oxidation initial potential of the device formed by them is closest to 0.68 V and photocurrent density is up to 0.94 mA cm^{-2} with an applied bias of 1.23 V vs. RHE (pH 8.0) under visible light irradiation. It can be seen from Figure 9b that the photocurrent of TiO_2 was improved after PEI/POMs multilayer films assembled. After modifying with (b-PEI-POM)n, onset potential and photocurrent density of TiO_2/b-PEI/Co_4PW_9 and$BiVO_4$/b-PEI/Co_4PW_9 are 0.48 V/-0.23 V and 1.96/0.105 mA cm^{-2}, respectively. The results are valuable for the introduction of LBL technology in photo-electrocatalysis.
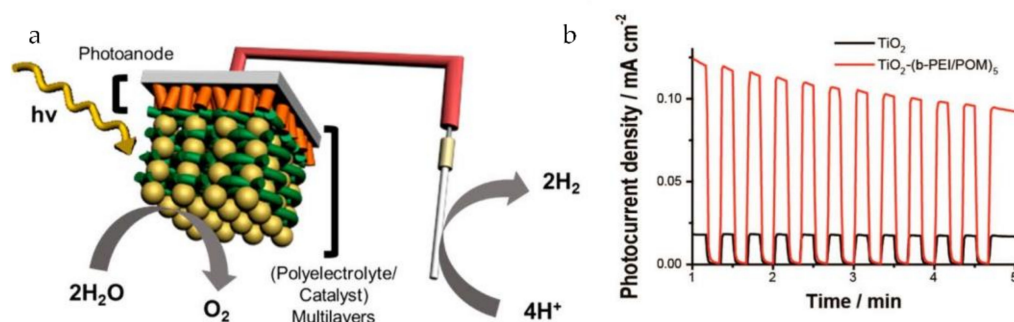
Figure 9. (**a**) The experimental procedure and the functional components used in this study is graphically illustrated. (**b**) TiO_2 photoanodes was studied by measuring LSV and photocurrent density with and without light irradiation. Reprinted with permission from [108]. Copyright (2017) American Chemical Society.

The LBL method uses electrostatic interaction and needs to introduce PE as a positive charge. However, PE is weakly conductive, which may affect the catalytic efficiency. In 2021, Yang et al. [110] prepared TiO_2 nanorods (NRs) FTO substrate by hydrothermal method, then refluxed with Co_4PW_9 composite material and dried to obtain Co_4PW_9/ TiO_2 NRs composite photo electrode, which excluded the influence of PE. When the applied voltage is 1.23 V (vs. RHE), the photocurrent density of Co_4PW_9/ TiO_2 NRS is 0.42 mA cm^{-2}, which is 1.2 times of the original TiO_2 NRs.

2.2.3. POMs Modified $BiVO_4$ Photo-Electrocatalyst

In 2017, Xu et al. [111] doped Keggin-type POMs such as $H_3PW_{12}O_{40}$ (PW_{12}) and $K_6[CoW_{12}O_{40}]$ (CoW_{12}) into n-type semiconductor $BiVO_{4\neg}$ to prepare the photoanodes, which were used for photocatalytic water oxidation. The measured data indicated that $BiVO_4$/POMs composite photoanodes exhibited higher photocatalytic performance than original $BiVO_4$ photoanode. As shown in Figure 10b, the enhanced performance was attributed to energy band matching between $BiVO_4$ and POMs to drive migrating of photogenic electrons from $BiVO_4$ to POMs, which was supported by photoluminescence spectra

and surface photovoltage measurements. This work represents the $BiVO_4$ based composite photoanode is an effective approach to improve the PEC water oxidation performance.
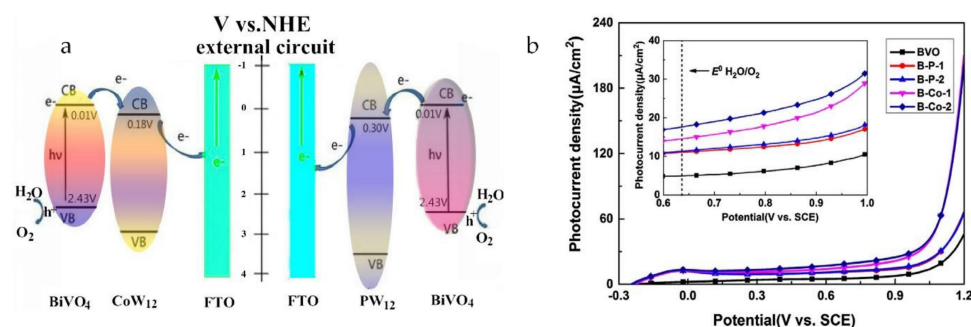

Figure 10. (**a**) Schematic illustrations of charge transfer processes for $BiVO_4/CoW_{12}$ and $BiVO_4/PW_{12}$ electrodes. (**b**) LSV plots of $BiVO_4$ photoanode, $BiVO_4/PW_{12}$ photoanode, and $BiVO_4/CoW_{12}$ photoanode measured in 0.1M Na_2SO_4 solution (pH 5.9) under visible light ($\lambda > 400$ nm, 100 mW/cm^2) tiny illumination from the front side, the inset is a magnified view of photocurrent curves at the range of 0.6–1.0 V [111].

In 2018, Kim et al. [112] used $[Co_4(H_2O)_2(VW_9O_{34})_2]^{10-}$ to modify $BiVO_4$ as a photoanode, and $[Ni_4(H_2O)_2(PW_9O_{34})_2]^{10-}$ to modify Cu_2O as a photocathode to form a photoelectrochemical cell for water decomposition into H_2 and O_2 using layer by layer assembly, as shown in Figure 11. The PEC cell exhibited a maximum incident photon-to-current conversion efficiency (IPCE) of 1.46% in the near-UV and blue-light spectral region. In 2019, the same group [113] further studied the kinetics of the catalytic water oxidation based on $[Co_4(H_2O)_2(VW_9O_{34})_2]^{10-}$ modified $BiVO_4$ ($Co_4VW_9/BiVO_4$) in the system above, and meanwhile studied how catalytic multilayers (CMs) technology improved the catalytic performance of $BiVO_4$. Based on the experimental investigation, it concludes that (1) CMs could improve charge separation/ transport in the bulk $BiVO_4$ because of the passivation of surface recombination centers; (2) CMs could increase efficient charge transport from the underlying $BiVO_4$ photoanode to Co_4VW_9 via hopping conduction due to nanoscale organization of PDDA and Co_4VW_9, and (3) CMs display outstanding catalytic activity. It is noteworthy here that the $BiVO_4$ photoanodes modified by CMs for solar water oxidation are reminiscent of the natural photosynthetic system, which can efficiently harvest sunlight and utilize photogenerated charge carriers, even with nonconducting components. The highest TOF for the prepared photoanode is 1.11×10^2 s^{-1}.
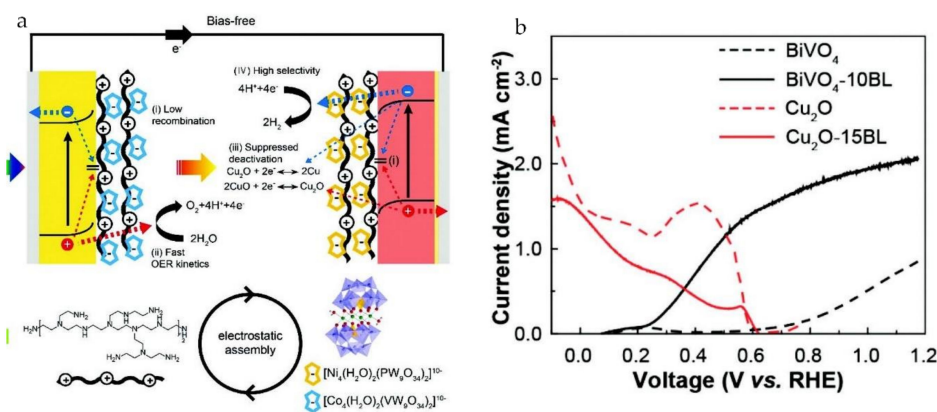
Figure 11. (**a**) Schematic illustrations explaining the inherent problems of a PEC cell composed of a Cu_2O photocathode and $BiVO_4$ photoanode. (**b**) LSV curves of the Cu_2O photocathodes and $BiVO_4$ photoanodes measured with and without the respective catalytic multilayers. [112].

Later scholars found that the improvement of photocatalysis by using cobalt poly-oxometalate (CoPOM) directly on $BiVO_4$ photoanode was limited. The main challenge was that the stability of CoPOM combined with semiconductor photoanode was not ideal. In order to solve this problem, adhesive polymers or molecular connectors are usually used. However, this will lead to poor conductivity, which will indirectly affect the catalytic efficiency. In 2020, Fan et al. [114] choose to use the good conductivity of carbon material to improve the catalytic properties of the material, as shown in Figure 12. N-doped carbon layer was grown in situ on BiVO4 photoanode, and CoPOM nanoparticles were deposited on it. CoPOM has a negative surface charge. In phosphate buffer solution, pyridine nitrogen adsorption makes H^+ ions form protonated n-doped sites with positive charge. Therefore, CoPOM and N-doped carbon can be assembled by electrostatic interaction. The conformal carbon layer is favorable for charge transfer and promotes the uniform distribution of CoPOM. The molecular catalyst CoPOM can significantly improve the efficiency of hole injection and obtain a lower initial potential, which is the characteristic of the real oxygen evolution catalyst. According to the PEC results of $BiVO_4$–N/C–CoPOM, the initial potential of $BiVO_4$–N/C–CoPOM photoanode is 240 mV higher than that of undoped $BiVO_4$ photoanode. Under AM 1.5 for 30 min, $BiVO_4$–N/C–CoPOM photoanode produces 10.1 µ mol/cm oxygen at 1.23 V vs. RHE, which corresponds to 84.4% Faraday efficiency. The photocurrent density of $BiVO_4$–N/C–CoPOM is 3.30 mA cm^{-2} at 1.23 V vs. RHE, which is 5.4-fold greater than that of the pristine $BiVO_4$. This is probably the best level in recent years. The cocatalyst effect of CoPOM and the improvement of charge injection efficiency are the main reasons for the improvement of PEC water oxidation performance. In addition, the maximum bias photon current efficiency (ABPE) of $BiVO_4$–N/C–CoPOM can be obtained at low potential, which is consistent with the linear sweep voltammetry (LSV) curve, which is conducive to the overall splitting of water in the two kinds of photoelectrode structures.
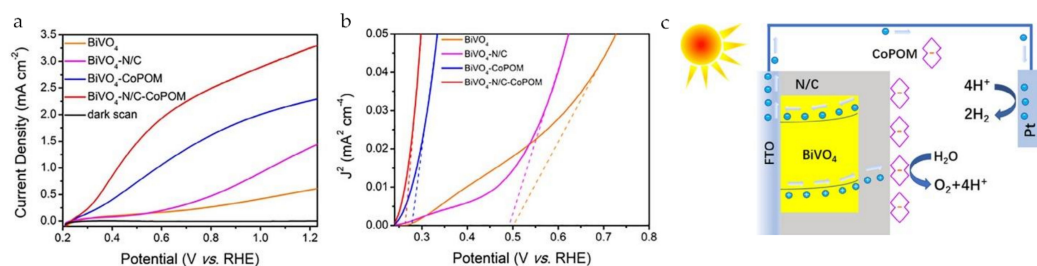
Figure 12. (**a**) PEC performances of $BiVO_4$, $BiVO_4$–N/C, $BiVO_4$–CoPOM, and $BiVO_4$–N/C–CoPOM. LSV curves under AM 1.5G illumination, (**b**) Bulter plots, and (**c**) Graphical abstract [114].

2.2.4. POMs Modified Other Semiconductors Photo-Electrocatalyst

In 2017, Xu et al. [96] fabricated a composite material containing Co_9S_8, TiO_2 and PW_{12} ($PW_{12}O_{40}{}^{3-}$) used as photoanode $TiO_2/Co_9S_8/PW_{12}$. The photoelectrochemical tests indicated that thus-prepared photoanode $TiO_2/Co_9S_8/PW_{12}$ showed enhanced photocurrent density compared with its components, as shown in Figure 13. Thus, this fabricated photoanode is expected to have good photoelectrochemical performance for the water oxidation. It can be seen that the photoanode $TiO_2/Co_9S_8/PW_{12}$ reaches the highest photoconversion efficiency comparing to that of its components, further confirming that the constructed photoanode $TiO_2/Co_9S_8/PW_{12}$ by introducing Co_9S_8 and PW_{12} into composite TiO_2 effectively increase the photoelectrochemical performance for water splitting, which is attributed to the synergistic effects of Co_9S_8 and PW_{12} on the composite TiO_2 as PW_{12} can promote charge separation whilst Co_9S_8 can act as a good mediator of electron transport.
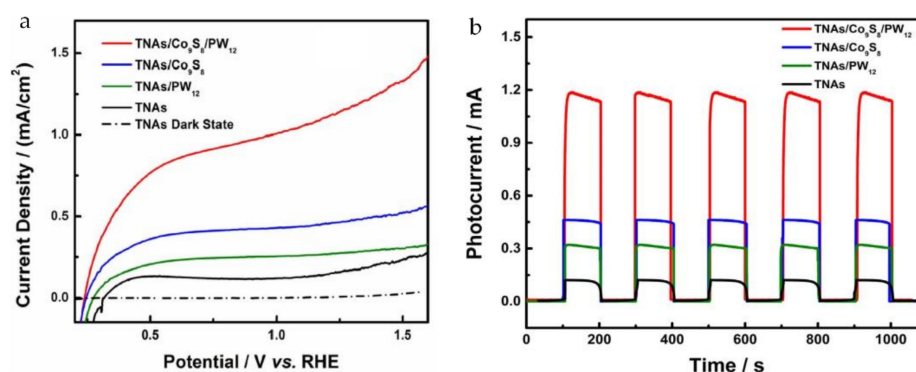
Figure 13. (**a**) LSV of TNAs, TNAs/PW_{12}, TNAs/Co_9S_8, and TNAs/Co_9S_8/PW_{12} the composite photoelectrodes in 0.5 M Na_2SO_4 Aqueous solution. (**b**) The Photocurrent responses of TNAs, TNAs/PW_{12}, TNAs/Co_9S_8, and TNAs/Co_9S_8/PW_{12} composite photoanodes [96].

In 2018, Jeon et al. [115] electrochemically deposited POM Ru_4SiW_{10} ([$Ru_4O_4(OH)_2(H_2O)_4(\gamma$-$SiW_{10}O_{36})_2$]$^{10-}$) and PPy on semiconductors. WO_3 was used to prepare a photoanode WO_3/PPy-Ru_4SiW_{10} by the electro-polymerization and co-deposition strategies. As well-known, the semiconductor WO_3 has good conductivity and long electron hole diffusion length, has lower band gaps and OER overpotentials and cheaper than TiO_2; however, it is easy to be corroded and deactivated in the presence of reactive oxygen species (such as hydrogen peroxide), thus, the uses of WO_3 alone is restricted during the water splitting. The authors prepared the composite photoanode WO_3/PPy-Ru_4SiW_{10} containing Ru_4SiW_{10} with good catalytic activity for the water oxidation and conductive polymer PPy with high efficiency of extinction could suppress the formation of hydrogen peroxide in the process of water oxidation. Therefore, the fabricated photoanode significantly improved the water oxidation performance under solar illumination.

As we all know, silicon is the most abundant element in the earth's crust except oxygen. In the meanwhile, silicon is also a semiconducting material with Eg 1.12 eV. This is one of the most promising photocathodes because of its abundance, biocompatibility, tunable electronic properties, and ability to harvest photons from a large portion of the solar spectrum. In 2019, Tourneur et al. [116] immobilized [$Mo_3S_4(H_2O)_9$]$^{4+}$/[$H_7P_8W_{48}O_{184}$]$^{33-}$ ([116,117]) cocatalyst onto a micro-structured p-type silicon with drop-casting procedure. Furthermore, [116,117] was electrostatically incorporated into poly(3,4-ethylenedioxythiophene) (PEDOT) film at the interface of a micropyramidal silicon (Si_{mPy}) photocathode. The production rate of H_2 for Si_{mPy}/[116,117] is ca. 100 μmol cm^{-2} h^{-1} at 0 V vs. RHE.

Table 2 lists POMs-based semiconductor compounds in PEC water splitting and is organized in a chronological format.

Table 2. Summary of POMs-based semiconductor compounds in PEC.

No.	Cocatalyst	Working Electrode	Electrolytes	Modification Methods	Light Source	Onset Potential (V vs. RHE)	Current Density (mA cm^{-2}) E=1.23V vs. RHE	The Reference(Year)
1	TiO_2/PW_{12} TiO_2/P_2Mo_{18} (methanol)	ITO	0.1M Na_2SO_4	LBL	6 W UV lamp (365 nm) 105 $\mu W \cdot cm^{-2}$	-	-	Sun et al. [95] (2010)
2	TiO_2/Ru_4PW_{10} TiO_2/Ru_4SiW_{10}	FTO	0.1 M KNO_3 (pH 10)	Silanization	150 W Xe (130 mW power at the quartz window).	-	ca. 1.2	Lauinger et al. [106] (2015)
3	$BiVO_4/PW_{12}$ $BiVO_4/CoW_{12}$	FTO	0.1M Na_2SO_4 (pH 5.9)	Doctor blade technique	400 W Xe lamp ($\lambda > 400$ nm, 100 mW/cm^{-2}	-	0.202 (1.2V vs. SCE)	Xi et al. [111] (2017)
4	$TNAs/Co_9S_8/PW_{12}$	Ti foil	0.5 M Na_2SO_4	Ionic layer adsorption and reaction (SILAR)	300 W Xe (100 mW cm^{-2})		1.12	Liu et al. [96] (2017)
5	Fe_2O_3/b-PEI/Co_4PW_9 TiO_2/b-PEI/Co_4PW_9 $BiVO_4$/b-PEI/Co_4PW_9	FTO	80 mM phosphate buffer (pH 8.0)	LBL	300 W Xe (100 mW cm^{-2})	0.68 0.48 −0.23	0.94 1.96 0.105	Jeon et al. [108,115,118] (2018)
8	$Si_{mPy}/$[117]	Si_{mPy}	1.0 M H_2SO_4 (pH 0.3)	Drop-casting and electrostatic incorporated	AM 1.5G, 100 mW cm^{-2}	0.33	-	Tourneur et al. [116] (2019)
9	$BiVO_4$-N/C-CoPOM	FTO	A 0.5 M phosphate buffer solution (pH 7) with/without 1 M Na_2SO_3	Electrodeposition and electrostatic interactions	A 300 W Xenon lamp with an AM 1.5G filter (100 mW cm^{-2})	0.26 V	3.30	Fan et al. [110,114] 2021)

3. Conclusions

Here, we summarize recent advances in the research of POMs and semiconductor materials in the following two aspects: the applications of POMs and semiconductor composites in the field of photocatalytic and photo-electrocatalytic water splitting. The different semiconductors such as TiO_2, CdS, Co_3O_4, C_3N_4, $BiVO_4$, etc. were modified by POMs to form the composite materials, which were used as photo-catalysts and photo-electrocatalysts for water splitting. The results show synergistic enhancement performance for water splitting, and POMs were proved to delay the recombination of photogenic electron hole pairs in semiconductor materials, affect the wavelength range of light absorption of the catalyst, and even stabilize the catalyst. Overall, this is an area with more potential and underexploited.

In this area, we still face some challenges: for example, it is a huge task to find and develop the most suitable POM from a great variety POMs for photocatalytic and photo-electrocatalytic water decomposition. Therefore, the following research should be carried out: first, according to the composition, structure and properties of POMs, the light absorption range of different POMs should be theoretically studied. The POMs have obvious absorption in ultraviolet range and it will be a great breakthrough that suitable semiconductor materials with POMs will be selected to adjust the absorbance range from ultraviolet visible range to continuous absorption in visible light to ultraviolet light. In addition, the combination of POMs with similar structure to the active centers PSII of green plants and semiconductors also has the potential to catalyze water-splitting. Although there are some theoretical and experimental studies on POM and semiconductor composites, it is still not systematic. The combination of theoretical research and experimental research is the best way to obtain ideal POM and semiconductor composites water-splitting catalyst. In order to mass-produce hydrogen production from water, it is necessary to improve the catalyst stability, repeatability, and catalytic activity in the future.

References

1. Pope, M.T.; Müller, A. Polyoxometalate chemistry: An old field with new dimensions in several disciplines. *Angew. Chem. Int. Ed.* **1991**, *30*, 34–48. [CrossRef]
2. Li, F.-C.; Tan, L.-K.; Li, X.-L.; Kong, H.-J.; Ge, L.-M.; Yue, L.-Y.; Han, L.F. Syntheses, structures and catalytic properties of Evans-Showell-type polyoxometalate-based 3D metal-organic complexes constructed from the semi-rigid bis(pyridylformyl)piperazine ligand and transition metals. *Dalton Trans.* **2019**, *48*, 5831–5841. [CrossRef] [PubMed]
3. Ismail, A.H. Synthesis and Structural Characterization of Lanthanide-Containing Polyoxometalates. Ph.D. Thesis, Jacobs University, Bremen, Germany, February 2011.
4. Salomon, W.; Roch-Marchal, C.; Mialane, P.; Rouschmeyer, P.; Serre, C.; Haouas, M.; Taulelle, F.; Yang, S.; Ruhlmann, L.; Dolbecq, A. Immobilization of polyoxometalates in the Zr-based metal organic framework UiO-67. *Chem. Commun.* **2015**, *51*, 2972–2975. [CrossRef] [PubMed]
5. Carraro, M.; Gross, S. Hybrid materials based on the embedding of organically modified transition metal oxoclusters or polyoxometalates into polymers for functional applications: A review. *Materials* **2014**, *7*, 3956–3989. [CrossRef]
6. Wang, M.; Dipazir, S.; Lu, P.; Wang, Y.; Yuan, M.; Li, S.; Zhang, G. Synthesis of polyoxometalates derived bifunctional catalyst towards efficient overall water splitting in neutral and alkaline medium. *J. Colloid Interface Sci.* **2018**, *532*, 774–781. [CrossRef]
7. Long, D.-L.; Tsunashima, R.; Cronin, L. Polyoxometalates: Building blocks for functional nanoscale systems. *Angew. Chem. Int. Ed.* **2010**, *49*, 1736–1758. [CrossRef]
8. Han, Q.; Ding, Y. Recent advances in the field of light-driven water oxidation catalyzed by transition-metal substituted polyoxometalates. *Dalton Trans.* **2018**, *47*, 8180–8188. [CrossRef]

9. Ammam, M. Polyoxometalates: Formation, structures, principal properties, main deposition methods and application in sensing. *J. Mater. Chem. A* **2013**, *1*, 6291–6312. [CrossRef]
10. Maya, F.; Paull, B. Recent strategies to enhance the performance of polymer monoliths for analytical separations. *J. Sep. Sci.* **2019**, *42*, 1564–1576. [CrossRef]
11. Roh, H.-S. Nanocatalysts for hydrogen production. *Catalysts* **2021**, *11*, 288. [CrossRef]
12. Rajan, A.G.; Martirez, J.M.P.; Carter, E.A. Why do we use the materials and operating conditions we use for heterogeneous (photo)electrochemical water splitting? *ACS Catal.* **2020**, *10*, 11177–11234. [CrossRef]
13. Shan, C.-H.; Zhang, H.; Chen, W.-L.; Su, Z.-M.; Wang, E.-B. Pure inorganic D–A type polyoxometalate/reduced graphene oxide nanocomposite for the photoanode of dye-sensitized solar cells. *J. Mater. Chem. A* **2016**, *4*, 3297–3303. [CrossRef]
14. Liu, Z.-J.; Wang, X.-L.; Qin, C.; Zhang, Z.-M.; Li, Y.-G.; Chen, W.-L.; Wang, E.-B. Polyoxometalate-assisted synthesis of transition-metal cubane clusters as artificial mimics of the oxygen-evolving center of photosystem II. *Coord. Chem. Rev.* **2016**, *313*, 94–110. [CrossRef]
15. Chuncheng, C.; Wei, Z.; Pengxiang, L.; Jincai, Z.; Nick, S. Photosensitized degradation of dyes in polyoxometalate solutions versus TiO2 dispersions under visible-light irradiation: Mechanistic implications. *Chem. A Eur. J.* **2010**, *10*, 1956–1965.
16. Park, H.; Choi, W. Photoelectrochemical investigation on electron transfer mediating behaviors of polyoxometalate in UV-illuminated suspensions of TiO2 and Pt/TiO2. *J. Phys. Chem. B* **2003**, *107*, 3885–3890. [CrossRef]
17. Gao, W.; Yu, T.; Du, Y.; Wang, R.; Wu, L.; Bi, L. First orange fluorescence composite film based on Sm-substituted tungstophosphate and its electrofluorochromic performance. *ACS Appl. Mater. Interfaces* **2016**, *8*, 11621–11628. [CrossRef]
18. Hill, C.L.; Bouchard, D.A. Catalytic photochemical dehydrogenation of organic substrates by polyoxometalates. *J. Am. Chem. Soc.* **1985**, *107*, 5148–5157. [CrossRef]
19. Liu, Y.; Liu, J.; Li, X. Progress in photocatalytic hydrogen production of semiconductors with d~(10) and d~0 electronic configuration. *Chemistry* **2013**, *76*, 969–975.
20. Li, L.; Guo, Y.; Zhou, P.; Yu, X.; Kang, W. Preparation of porous H3PW12O40/TiO2 and its photocatalytic activity for degradation of aqueous dyes under visible-light. *Chin. J. Catal.* **2005**, *26*, 209–215.
21. Friesen, D.A.; Headley, J.V.; Langford, C.H. The photooxidative degradation of N-Methylpyrrolidinone in the presence of Cs3PW12O40and TiO2Colloid photocatalysts. *Environ. Sci. Technol.* **1999**, *33*, 3193–3198. [CrossRef]
22. Tada, H.; Hyodo, M.; Kawahara, H. photoinduced polymerization of 1,3,5,7-tetramethylcyclotetrasiloxane by titania particles. *J. Phys. Chem.* **1991**, *95*, 10185–10188. [CrossRef]
23. Wang, D.; Ma, R. Preparation of nanocomposite α-SiW11Ti/PANI/TiO2 and photocatalytic performance. In Proceedings of the 5th National Polyoxometalates Chemistry Symposium of the Chinese Chemical Society, Harbin, China, 15 July 2013.
24. Shi, H.; Yu, Y.; Zhang, Y.; Feng, X.; Zhao, X.; Tan, H.; Khan, S.U.; Li, Y.; Wang, E. Polyoxometalate/TiO2/Ag composite nanofibers with enhanced photocatalytic performance under visible light. *Appl. Catal. B Environ.* **2018**, *221*, 280–289. [CrossRef]
25. Zhang, P.; Yu, G.; Jiang, Z. Advances in semiconductor photocatalysts and their modification. *Adv. Environ. Sci.* **1997**, *5*, 2–11.
26. Henderson, M.A. A surface science perspective on TiO2 photocatalysis. *Surf. Sci. Rep.* **2011**, *66*, 185–297. [CrossRef]
27. Kukovecz, Á.; Kordás, K.; Kiss, J.; Kónya, Z. Atomic scale characterization and surface chemistry of metal modified titanate nanotubes and nanowires. *Surf. Sci. Rep.* **2016**, *71*, 473–546. [CrossRef]
28. Li, Y.; Lu, G.; Li, S. Advances in semiconductor photocatalytic decomposition of water. *J. Mol. Catal.* **2001**, *15*, 72–79.
29. Hagfeldt, A.; Graetzel, M. Light-induced redox reactions in nanocrystalline systems. *Chem. Rev.* **1995**, *95*, 49–68. [CrossRef]
30. Kudo, A.; Miseki, Y. Heterogeneous photocatalyst materials for water splitting. *Chem. Soc. Rev.* **2009**, *38*, 253–278. [CrossRef]
31. Arunachalam, P.; Nagai, K.; Amer, M.S.; Ghanem, M.A.; Ramalingam, R.J.; Al-Mayouf, A.M. Recent developments in the use of heterogeneous semiconductor photocatalyst based materials for a visible-light-induced water-splitting system—A brief review. *Catalysts* **2021**, *11*, 160. [CrossRef]
32. Gopidas, K.R.; Bohorquez, M.; Kamat, P.V. Photophysical and photochemical aspects of coupled semiconductors: Charge-transfer processes in colloidal cadmium sulfide-titania and cadmium sulfide-silver(I) iodide systems. *J. Phys. Chem.* **1990**, *94*, 6435–6440. [CrossRef]
33. Brus, L.E. A simple model for the ionization potential, electron affinity, and aqueous redox potentials of small semiconductor crystallites. *J. Chem. Phys.* **1983**, *79*, 5566–5571. [CrossRef]
34. Brus, L.E. Electron—electron and electron-hole interactions in small semiconductor crystallites: The size dependence of the lowest excited electronic state. *J. Chem. Phys.* **1984**, *80*, 4403–4409. [CrossRef]
35. Rossetti, R.; Ellison, J.L.; Gibson, J.M.; Brus, L.E. Size effects in the excited electronic states of small colloidal CdS crystallites. *J. Chem. Phys.* **1984**, *80*, 4464. [CrossRef]
36. Wang, C.M.; Heller, A.; Gerischer, H. Palladium catalysis of O2 reduction by electrons accumulated on TiO2 particles during photoassisted oxidation of organic compounds. *J. Am. Chem. Soc.* **1992**, *114*, 5230–5234. [CrossRef]
37. Escudero, J.; Cervera-March, S.; Gimenez, J.; Simarro, R. Physical characteristics of photocatalysts affecting the performance of a process in a continuous photoreactor. *Sol. Energy Mater.* **1988**, *17*, 151–163. [CrossRef]
38. Gao, Y.-M.; Lee, W.; Trehan, R.; Kershaw, R.; Dwight, K.; Wold, A. Improvement of photocatalytic activity of titanium (IV) oxide by dispersion of Au on TiO2. *Mater. Res. Bull.* **1991**, *26*, 1247–1254. [CrossRef]
39. Kondo, M.M.; Jardim, W.F. Photodegradation of chloroform and urea using Ag-loaded titanium dioxide as catalyst. *Water Res.* **1991**, *25*, 823–827. [CrossRef]

40. Rufus, I.B.; Ramakrishnan, V.; Viswanathan, B.; Kuriacose, J.C. Rhodium and rhodium sulfide coated cadmium sulfide as a photocatalyst for photochemical decomposition of aqueous sulfide. *Langmuir* **1990**, *6*, 565–567. [CrossRef]

41. Choi, W.; Termin, A.; Hoffmann, M.R. The Role of metal ion dopants in quantum-sized TiO2: Correlation between photoreactivity and charge carrier recombination dynamics. *J. Phys. Chem.* **1994**, *98*, 13669–13679. [CrossRef]

42. Milis, A.; Peral, J.; Domènech, X.; Navío, J. Heterogeneous photocatalytic oxidation of nitrite over iron-doped TiO2 samples. *J. Mol. Catal.* **1994**, *87*, 67–74. [CrossRef]

43. Hong, A.P.; Bahnemann, D.W.; Hoffmann, M.R. Cobalt(II) tetrasulfophthalocyanine on titanium dioxide. 2. Kinetics and mechanisms of the photocatalytic oxidation of aqueous sulfur dioxide. *J. Phys. Chem.* **1987**, *91*, 6245–6251. [CrossRef]

44. Uchihara, T.; Matsumura, M.; Ono, J.; Tsubomura, H. Effect of EDTA on the photocatalytic activities and flatband potentials of cadmium sulfide and cadmium selenide. *J. Phys. Chem.* **1990**, *94*, 415–418. [CrossRef]

45. Han, N.C.; Cho, S.H.; Lee, W.Y. Electrogenerated chemiluminescence from tris(2,2 '-bipyridyl)ruthenium(II) immobilized in titania-perfluorosulfonated Ionomer composite films. *Anal. Chem.* **2003**, *75*, 4250–4256.

46. Shi, H.; Li, N.; Sun, Z.; Wang, T.; Xu, L. Interface modification of titanium dioxide nanoparticles by titanium-substituted polyoxometalate doping for improvement of photoconductivity and gas sensing applications. *J. Phys. Chem. Solids* **2018**, *120*, 57–63. [CrossRef]

47. Wu, X.; Zhang, X.; Zhao, S.; Gong, Y.; Djellabi, R.; Lin, S.; Zhao, X. Highly-efficient photocatalytic hydrogen peroxide production over polyoxometalates covalently immobilized onto titanium dioxide. *Appl. Catal. A Gen.* **2020**, *591*, 117271. [CrossRef]

48. Hiskia, A.; Mylonas, A.; Papaconstantinou, E. Comparison of the photoredox properties of polyoxometallates and semiconducting particles. *Chem. Soc. Rev.* **2000**, *30*, 62–69. [CrossRef]

49. Zouni, A.; Witt, H.-T.; Kern, J.; Fromme, P.; Krauss, N.; Saenger, W.; Orth, P.P. Crystal structure of photosystem II from Synechococcus elongatus at 3.8 Å resolution. *Nat. Cell Biol.* **2001**, *409*, 739–743.

50. Sun, Z.; Chen, H.; Huang, Q.; Du, P. Enhanced photocatalytic hydrogen production in water under visible light using noble metal-free ferrous phosphide as an active cocatalyst. *Catal. Sci. Technol.* **2015**, *5*, 4964–4967. [CrossRef]

51. Sun, Z.; Liu, X.; Yue, Q.; Jia, H.; Du, P. Cadmium sulfide nanorods decorated with copper sulfide via one-step cation exchange approach for enhanced photocatalytic hydrogen evolution under visible light. *ChemCatChem* **2015**, *8*, 157–162. [CrossRef]

52. Li, Y.; Yao, R.; Chen, Y.; Xu, B.; Chen, C.; Zhang, C. Mimicking the catalytic center for the water-splitting reaction in photosystem II. *Catalysts* **2020**, *10*, 185. [CrossRef]

53. Wang, S.-S.; Yang, G.-Y. Recent advances in polyoxometalate-catalyzed reactions. *Chem. Rev.* **2015**, *115*, 4893–4962. [CrossRef] [PubMed]

54. Fountaine, K.T.; Lewerenz, H.J.; Atwater, H.A. Efficiency limits for photoelectrochemical water-splitting. *Nat. Commun.* **2016**, *7*, 13706. [CrossRef] [PubMed]

55. Yoon, M.; Chang, J.A.; Kim, A.Y.; Choi, J.R.; Kim, K.; Lee, S.J. Heteropoly acid-incorporated TiO2Colloids as novel photocatalytic systems resembling the photosynthetic reaction center. *J. Phys. Chem. B* **2001**, *105*, 2539–2545. [CrossRef]

56. Gu, C.; Shannon, C. Investigation of the photocatalytic activity of TiO2—polyoxometalate systems for the oxidation of methanol. *J. Mol. Catal. A Chem.* **2007**, *262*, 185–189. [CrossRef]

57. Ciamician, G. The photochemistry of the future. *Science* **1912**, *36*, 385–394. [CrossRef] [PubMed]

58. Zou, Z.; Ye, J.; Sayama, K.; Arakawa, H. Direct splitting of water under visible light irradiation with an oxide semiconductor photocatalyst. *Nat. Cell Biol.* **2001**, *414*, 625–627. [CrossRef] [PubMed]

59. Esswein, A.J.; Nocera, D.G. Hydrogen production by molecular photocatalysis. *Chem. Rev.* **2007**, *107*, 4022–4047. [CrossRef]

60. Ravelli, D.; Dondi, D.; Fagnoni, M.; Albini, A. Photocatalysis. A multi-faceted concept for green chemistry. *Chem. Soc. Rev.* **2009**, *38*, 1999–2011. [CrossRef]

61. Anpo, M.; Kamat, P.V. *Environmentally Benign Photocatalysts*; Springer: New York, NY, USA, 2010.

62. Hagfeldt, A.; Boschloo, G.; Sun, L.; Kloo, L.; Pettersson, H. Dye-sensitized solar cells. *Chem. Rev.* **2010**, *110*, 6595–6663. [CrossRef]

63. Dolbecq, A.; Mialane, P.; Keita, B.; Nadjo, L. Polyoxometalate-based materials for efficient solar and visible light harvesting: Application to the photocatalytic degradation of azo dyes. *J. Mater. Chem.* **2012**, *22*, 24509–24521. [CrossRef]

64. Sartorel, A.; Carraro, M.; Toma, F.M.; Prato, M.; Bonchio, M. Shaping the beating heart of artificial photosynthesis: Oxygenic metal oxide nano-clusters. *Energy Environ. Sci.* **2012**, *5*, 5592–5603. [CrossRef]

65. Streb, C. New trends in polyoxometalate photoredox chemistry: From photosensitisation to water oxidation catalysis. *Dalton Trans.* **2011**, *41*, 1651–1659. [CrossRef]

66. Sartorel, A.; Bonchio, M.; Campagna, S.; Scandola, F. Tetrametallic molecular catalysts for photochemical water oxidation. *Chem. Soc. Rev.* **2013**, *42*, 2262–2280. [CrossRef]

67. Sarina, S.; Zhu, H.; Zheng, Z.; E Bottle, S.; Chang, J.; Ke, X.; Zhao, J.-C.; Huang, Y.; Sutrisno, A.; Willans, M.; et al. Driving selective aerobic oxidation of alkyl aromatics by sunlight on alcohol grafted metal hydroxides. *Chem. Sci.* **2012**, *3*, 2138–2146. [CrossRef]

68. Hammarstr, L.; Hammes-Schiffer, S. Artificial photosynthesis and solar fuels. *Acc. Chem. Res.* **2009**, *42*, 1859–1860. [CrossRef]

69. Lewis, N.S.; Nocera, D.G. Powering the planet: Chemical challenges in solar energy utilization. *Proc. Natl. Acad. Sci. USA* **2006**, *103*, 15729–15735. [CrossRef]

70. Barber, J. Photosynthetic energy conversion: Natural and artificial. *Chem. Soc. Rev.* **2008**, *38*, 185–196. [CrossRef]

71. Holger, D.; Ivelina, Z. Principles, efficiency, and blueprint character of solar-energy conversion in photosynthetic water oxidation. *Cheminform* **2010**, *41*, 1861–1870.

72. Zhang, C.; Chen, C.; Dong, H.; Shen, J.-R.; Dau, H.; Zhao, J. A synthetic Mn4Ca-cluster mimicking the oxygen-evolving center of photosynthesis. *Science* **2015**, *348*, 690–693. [CrossRef]

73. Liu, X.; Wang, F. Transition metal complexes that catalyze oxygen formation from water: 1979–2010. *Coord. Chem. Rev.* **2012**, *256*, 1115–1136. [CrossRef]

74. Lv, H.; Geletii, Y.V.; Zhao, C.; Vickers, J.W.; Zhu, G.; Luo, Z.; Song, J.; Lian, T.; Musaev, D.G.; Hill, C.L. Polyoxometalate water oxidation catalysts and the production of green fuel. *Chem. Soc. Rev.* **2012**, *41*, 7572–7589. [CrossRef] [PubMed]

75. Puntoriero, F.; Sartorel, A.; Orlandi, M.; La Ganga, G.; Serroni, S.; Bonchio, M.; Scandola, F.; Campagna, S. Photoinduced water oxidation using dendrimeric Ru(II) complexes as photosensitizers. *Coord. Chem. Rev.* **2011**, *255*, 2594–2601. [CrossRef]

76. Romain, S.; Vigara, L.; Llobet, A. Oxygen—oxygen bond formation pathways promoted by ruthenium complexes. *Accounts Chem. Res.* **2009**, *42*, 1944–1953. [CrossRef] [PubMed]

77. Ryu, J.; Nam, D.H.; Lee, S.H.; Park, C.B. Biocatalytic photosynthesis with water as an electron donor. *Chem. A Eur. J.* **2014**, *20*, 12020–12025. [CrossRef]

78. Singh, A.; Spiccia, L. Water oxidation catalysts based on abundant 1st row transition metals. *Coord. Chem. Rev.* **2013**, *257*, 2607–2622. [CrossRef]

79. Tsai, M.K.; Rochford, J.; Polyansky, D.E.; Wada, T.; Tanaka, K.; Fujita, E.; Muckerman, J.T. Characterization of redox states of Ru(OH2)(Q)(tpy)2+ (Q = 3,5-di-tert-butyl-1,2-benzoquinone, tpy = 2,2′:6′,2″-terpyridine) and related species through experimental and theoretical studies. *Inorg. Chem.* **2009**, *48*, 4372–4383. [CrossRef]

80. Stracke, J.J.; Finke, R.G. Distinguishing homogeneous from heterogeneous water oxidation catalysis when beginning with polyoxometalates. *ACS Catal.* **2014**, *4*, 909–933. [CrossRef]

81. Orlandi, M.; Argazzi, R.; Sartorel, A.; Carraro, M.; Scorrano, G.; Bonchio, M.; Scandola, F. Ruthenium polyoxometalate water splitting catalyst: Very fast hole scavenging from photogenerated oxidants. *Chem. Commun.* **2010**, *46*, 3152–3154. [CrossRef]

82. Liu, X.; Li, Y.; Peng, S.; Lu, G.; Li, S. Photosensitization of SiW11O398−-modified TiO2 by Eosin Y for stable visible-light H2 generation. *Int. J. Hydrogen Energy* **2013**, *38*, 11709–11719. [CrossRef]

83. Han, Z.G.; Bond, A.M.; ZHAO, C. Recent trends in the use of polyoxometalate-based material for efficient water oxidation. *Sci. China* **2011**, *54*, 1877–1887. [CrossRef]

84. Ensafi, A.A.; Heydari-Soureshjani, E.; Rezaei, B. Nanostructure polyoxometalates containing Co, Ni, and Cu as powerful and stable catalysts for hydrogen evolution reaction in acidic and alkaline solutions. *Int. J. Hydrog. Energy* **2017**, *42*, 5026–5034. [CrossRef]

85. Du, Y.; Yu, T.; Fu, Z.; Bi, L. A multilayer assembly of two mixed-valence Mn16-containing polyanions and study of their electrocatalytic activities towards water oxidation. *Dalton Trans.* **2018**, *47*, 7282–7289. [CrossRef]

86. Xing, X.; Liu, R.; Yu, X.; Zhang, G.; Cao, H.; Yao, J.; Ren, B.; Jiang, Z.; Zhao, H. Self-assembly of CdS quantum dots with polyoxometalate encapsulated gold nanoparticles: Enhanced photocatalytic activities. *J. Mater. Chem. A* **2013**, *1*, 1488–1494. [CrossRef]

87. Liu, M.; Li, F.; Sun, Z.; Xu, L.; Song, Y.; Munventwali, A. Enhanced photocatalytic H2evolution on CdS with cobalt polyoxo-tungstosilic and MoS2/graphene as noble-metal-free dual co-catalysts. *RSC Adv.* **2015**, *5*, 47314–47318. [CrossRef]

88. Bu, Y.; Zhang, Y.; Luo, X.; Li, F.; Liu, R.; Xu, L. Immobilizing CdS nanoparticles and MoS 2 /RGO on Zr-based metal—organic framework 12-tungstosilicate@UiO-67 toward enhanced photocatalytic H 2 evolution. *RSC Adv.* **2016**, *6*, 40560–40566. [CrossRef]

89. Zhai, X.-L.; Liu, J.; Hu, L.-Y.; Bao, J.-C.; Lan, Y.-Q. Polyoxometalate-decorated g-C3N4 -wrapping snowflake-like CdS nanocrystal for enhanced photocatalytic hydrogen evolution. *Chem. A Eur. J.* **2018**, *24*, 15930–15936. [CrossRef]

90. Lan, Q.; Zhang, Z.-M.; Qin, C.; Wang, X.-L.; Li, Y.-G.; Tan, H.-Q.; Wang, E.-B. Highly dispersed polyoxometalate-doped porous co3o4water oxidation photocatalysts derived from POM@MOF crystalline materials. *Chem. A Eur. J.* **2016**, *22*, 15513–15520. [CrossRef]

91. Maeda, K.; Wang, X.; Nishihara, Y. Photocatalytic activities of graphitic carbon nitride powder for water reduction and oxidation under visible light. *J. Phys. Chem. C* **2009**, *113*, 4940–4947. [CrossRef]

92. Yan, G.; Feng, X.; Xiao, L.; Xi, W.; Tan, H.; Shi, H.; Wang, Y.; Li, Y. Tuning of the photocatalytic performance of g-C3N4 by polyoxometalates under visible light. *Dalton Trans.* **2017**, *46*, 16019–16024. [CrossRef]

93. Zhang, Z.; Lin, Q.; Kurunthu, D.; Wu, T.; Zuo, F.; Zheng, S.-T.; Bardeen, C.J.; Bu, X.; Feng, P. synthesis and photocatalytic properties of a new heteropolyoxoniobate compound: K10[Nb2O2(H2O)2][SiNb12O40]·12H2O. *J. Am. Chem. Soc.* **2011**, *133*, 6934–6937. [CrossRef]

94. Dong, Y.; Han, Q.; Ma, K.; Song, F.; Zheng, S.; Ding, Y. Study two kind different catalytic behaviors for K4H1.2[Co0.6(H2O)0.6SiW11.4O39.4]-cocatalyzed visible light driven water oxidation in pH 1–7 media. *J. Catal.* **2020**, *392*, 29–38. [CrossRef]

95. Sun, Z.; Xu, L.; Guo, W.; Xu, B.; Liu, S.; Li, F. Enhanced photoelectrochemical performance of nanocomposite film fabricated by self-assembly of titanium dioxide and polyoxometalates. *J. Phys. Chem. C* **2010**, *114*, 5211–5216. [CrossRef]

96. Liu, R.; Sun, Z.; Song, X.; Zhang, Y.; Xu, L.; Xi, L. Toward non-precious nanocomposite photocatalyst: An efficient ternary photoanode TiO 2 nanotube/Co 9 S 8 /polyoxometalate for photoelectrochemical water splitting. *Appl. Catal. A Gen.* **2017**, *544*, 137–144. [CrossRef]

97. Fuel Cell Technologies. Fuel Cell Technologies Office Multi-Year Research, Development, and Demonstration Plan: Production Section. 2015. Available online: https://www.energy.gov/eere/fuelcells/downloads/fuelcell-technologies-office-multi-year-research-development-and-22 (accessed on 4 September 2020).

98. Guo, Y.; Hu, C. Heterogeneous photocatalysis by solid polyoxometalates. *J. Mol. Catal. A Chem.* **2007**, *262*, 136–148. [CrossRef]
99. Sivakumar, R.; Thomas, J.; Yoon, M. Polyoxometalate-based molecular/nano composites: Advances in environmental remediation by photocatalysis and biomimetic approaches to solar energy conversion. *J. Photochem. Photobiol. C Photochem. Rev.* **2012**, *13*, 277–298. [CrossRef]
100. Wang, T.; Sun, Z.; Li, F.; Xu, L. Nanostructured polyoxometalate-modified SnO 2 photoanode with improved photoelectrochemical performance. *Electrochem. Commun.* **2014**, *47*, 45–48. [CrossRef]
101. Wang, T.; Sun, Z.; Shi, H.; Xu, L. Enhanced photovoltaic response of Cu2ZnSnS4 thin film by polyoxometalate doping for solar cell application. *Thin Solid Films* **2018**, *664*, 130–135. [CrossRef]
102. Huang, B.; Hart, J.N. DFT study of various tungstates for photocatalytic water splitting. *Phys. Chem. Chem. Phys.* **2020**, *22*, 1727–1737. [CrossRef]
103. Luo, X.; Li, F.; Xu, B.; Sun, Z.; Xu, L. Enhanced photovoltaic response of the first polyoxometalate-modified zinc oxide photoanode for solar cell application. *J. Mater. Chem.* **2012**, *22*, 15050. [CrossRef]
104. Xiang, X.; Fielden, J.; Rodríguez-Córdoba, W.; Huang, Z.; Zhang, N.; Luo, Z.; Musaev, D.G.; Lian, T.; Hill, C.L. electron transfer dynamics in semiconductor—chromophore—polyoxometalate catalyst photoanodes. *J. Phys. Chem. C* **2013**, *117*, 918–926. [CrossRef]
105. Fielden, J.; Sumliner, J.M.; Han, N.; Geletii, Y.V.; Xiang, X.; Musaev, D.G.; Lian, T.; Hill, C.L. Water splitting with polyoxometalate-treated photoanodes: Enhancing performance through sensitizer design. *Chem. Sci.* **2015**, *6*, 5531–5543. [CrossRef]
106. Lauinger, S.M.; Sumliner, J.M.; Yin, Q.; Xu, Z.; Liang, G.; Glass, E.N.; Lian, T.; Hill, C.L. High Stability of Immobilized Polyoxometalates on TiO2Nanoparticles and Nanoporous Films for Robust, Light-Induced Water Oxidation. *Chem. Mater.* **2015**, *27*, 5886–5891. [CrossRef]
107. Ren, Z. Study of Functional Composites Based on Polyoxometalates and Graphene. Master Thesis, Northeast Normal University, Changchun, China, 2016. (In Chinese).
108. Jeon, D.; Kim, H.; Lee, C.; Han, Y.; Gu, M.; Kim, B.-S.; Ryu, J. Layer-by-Layer Assembly of Polyoxometalates for Photoelectrochemical (PEC) Water Splitting: Toward Modular PEC Devices. *ACS Appl. Mater. Interfaces* **2017**, *9*, 40151–40161. [CrossRef]
109. Mishra, M.; Chun, D.-M. α-Fe 2 O 3 as a photocatalytic material: A review. *Appl. Catal. A Gen.* **2015**, *498*, 126–141. [CrossRef]
110. Yang, P.; Liu, Q.; Yu, F.; Wu, J.; Liu, Z.; Peng, B. Cobalt substituted polyoxophosphomolybdate modified TiO2 for boosted photoelectrocatalytic water oxidation. *J. Alloy. Compd.* **2021**, *854*, 157232. [CrossRef]
111. Xi, L.; Jin, Z.; Sun, Z.; Liu, R.; Xu, L. Enhanced photoelectrocatalytic performance for water oxidation by polyoxometalate molecular doping in BiVO 4 photoanodes. *Appl. Catal. A Gen.* **2017**, *536*, 67–74. [CrossRef]
112. Kim, H.; Bae, S.; Jeon, D.; Ryu, J. Fully solution-processable Cu2O—BiVO4 photoelectrochemical cells for bias-free solar water splitting. *Green Chem.* **2018**, *20*, 3732–3742. [CrossRef]
113. Bae, S.; Kim, H.; Jeon, D.; Ryu, J. Catalytic Multilayers for Efficient Solar Water Oxidation through Catalyst Loading and Surface-State Passivation of BiVO4 Photoanodes. *ACS Appl. Mater. Interfaces* **2019**, *11*, 7990–7999. [CrossRef]
114. Fan, K.; Chen, H.; He, B.; Yu, J. Cobalt polyoxometalate on N-doped carbon layer to boost photoelectrochemical water oxidation of BiVO4. *Chem. Eng. J.* **2020**, *392*, 123744. [CrossRef]
115. Jeon, D.; Kim, N.; Bae, S.; Han, Y.; Ryu, J. WO3/Conducting Polymer Heterojunction Photoanodes for Efficient and Stable Photoelectrochemical Water Splitting. *ACS Appl. Mater. Interfaces* **2018**, *10*, 8036–8044. [CrossRef]
116. Tourneur, J.; Fabre, B.; Loget, G.; Vacher, A.; Mériadec, C.; Ababou-Girard, S.; Gouttefangeas, F.; Joanny, L.; Cadot, E.; Haouas, M.; et al. Molecular and material engineering of photocathodes derivatized with polyoxometalate-supported {Mo3S4} HER catalysts. *J. Am. Chem. Soc.* **2019**, *141*, 11954–11962. [CrossRef]
117. Bao, Y.-Y.; Bi, L.-H.; Wu, L.-X. One-step synthesis and stabilization of gold nanoparticles and multilayer film assembly. *J. Solid State Chem.* **2011**, *184*, 546–556. [CrossRef]
118. Li, J.; Wang, L.; You, W.; Liu, M.; Zhang, L.; Sang, X. Catalytic effects of [Ag(H2O)(H3PW11O39)]3− on a TiO2 anode for water oxidation. *Chin. J. Catal.* **2018**, *39*, 534–541. [CrossRef]